IEEE Access
Multidisciplinary ⋮ Rapid Review ⋮ Open Access Journal

Received 6 April 2024, accepted 26 April 2024, date of publication 6 May 2024, date of current version 13 May 2024.

Digital Object Identifier 10.1109/ACCESS.2024.3396998

RESEARCH ARTICLE

Dual-Band Bandpass Filters Using 3D Printed Dual-Mode Nested Spherical Resonators

JIAWEI LIU[1,2], (Graduate Student Member, IEEE), AND DIMITRA PSYCHOGIOU[2,3], (Senior Member, IEEE)

[1]School of Electronic Science and Engineering, University of Electronic Science and Technology of China, Chengdu 611731, China
[2]Tyndall National Institute, Cork, T12 R5CP Ireland
[3]School of Engineering, University College Cork, Cork, T12 K8AF Ireland

Corresponding author: Jiawei Liu (liujwgyem@std.uestc.edu.cn)

This work was supported in part by the Science Foundation Ireland (SFI) under Grant 20/RP/8334, and in part by China Scholarship Council (CSC).

ABSTRACT This paper reports on a new class of 3D additively-manufactured dual-band bandpass filters (BPFs). They are based on miniaturized dual-mode nested-spherical resonators which consist of two post-supported metallic spheres that load a hollow spherical cavity and give rise to two independently-controlled resonant modes. The two modes can be exploited for the realization of dual-band BPFs with two independently-controlled bands in terms of frequency and bandwidth. The four transmission zeros (TZs) also can be controlled which give rise to better stopband response. To validate the filter concept, a dual-band BPF was designed, manufactured and measured. It exhibited, two passbands centered at 1.5 GHz and 2.47 GHz with fractional bandwidths (FBWs) of 8.13 and 2.87 %, in-band insertion loss (IL) of 0.14 and 0.39 dB, and effective Q factor (Q_{eff}) of 1,448 and 2,088 respectively. The measured and simulated results have a good agreement. A low-cost and compact monolithic integration concept enabled by stereolithography apparatus (SLA) additive manufacturing is also demonstrated.

INDEX TERMS Additive manufacturing (AM), bandpass filters (BPFs), dual-band filter, low-loss filter, RF-filter.

I. INTRODUCTION

Emerging communication applications such as 5G and Internet of Space (IoS) are increasingly calling for RF transceivers able to support multiple bands and modes of operation while exhibiting the smallest possible physical size and weight. To facilitate size compactness while enabling multi-band operability, bandpass filters (BPFs) able to operate in multiple bands are currently being explored with dual-band configurations being among the most popular ones [1], [2], [3], [4], [5], [6], [7], [8], [9], [10].

For RF applications where, low insertion loss (IL) or high RF power handling is required, 3D RF dual-band filters such as those based on computer numerical control (CNC)-machined 3D metallic waveguides [1], [2], [3], and coaxial cavity resonators [4], [5], [6] are typically preferred due to their high unloaded quality-factor (Q) and high RF power handling characteristics. However, these configurations are bulky and expensive with the majority of the CNC-machined 3D dual-band BPFs being realized by multi-part assemblies using screws and fixtures that increase the cost and weight and add radiation loss.

Additive manufacturing (AM) techniques (or 3D printing) have been increasingly explored for manufacturing 3D resonators-based microwave dual-band BPFs, such as the spherical resonator-based configuration in [7], the ellipsoidal resonator-based in geometry in [8], and the coaxial resonator-based dual-band BPFs in [13] and [14]. Compared to traditional CNC machining techniques, AM facilitates filters with higher geometrical complexity and is potentially suitable for monolithic 3D integration. Various examples of monolithically-integrated 3D printed BPFs

The associate editor coordinating the review of this manuscript and approving it for publication was Photos Vryonides.

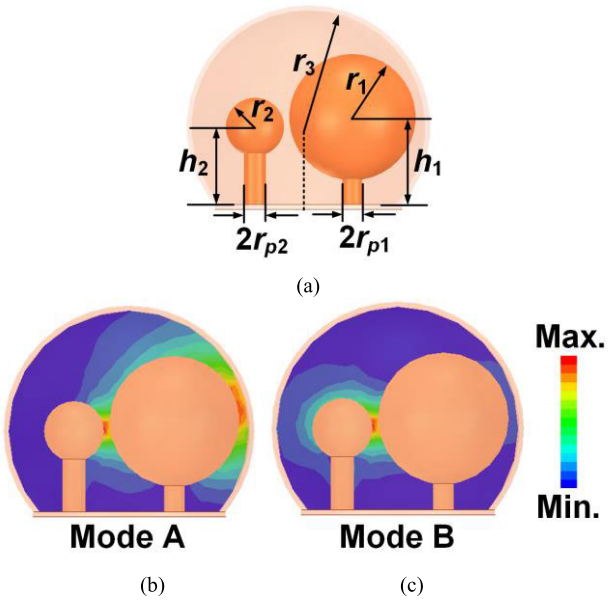

FIGURE 1. (a) Geometrical configuration of the dual-mode nested-spherical resonator having two independently-controlled modes (Mode A, B) within the same air-filled cavity. E-field of (b) Mode A (f = 1.27 GHz) and (c) of Mode B (f = 2.1 GHz).

TABLE 1. Comparison between the nested spherical resonator and the conventional hollow spherical resonator.

Type	Nested spherical (r_3=24 mm)				Conventional spherical (r_3=24 mm)			
Mode	1	2	3	4	1	2	3	4
Frequency	1.27	2.1	3.71	4.51	5.50	5.50	5.50	7.76
Q	2,127	3,522	6,693	5,042	19,409	19,413	19,441	18,825

have been shown to date [9], [10], [11], [12], [13], [14] and have demonstrated improved performance, smaller size and weight than their CNC-machined counter parts. However, to the best of the author's knowledge, monolithic AM-based integration concepts haven't been demonstrated for multi-band nested spherical BPFs with the exception of the work [13], [14] which however is focused on coaxial resonators where dual posts were used for the realization of dual-band BPFs and the concepts in [15] and [16] which is focused on conventional cylindrical and spherical resonators.

Considering the merits of AM and the need for compact high-Q dual-band BPFs in terrestrial 5G base stations, in emerging instrumentation systems and in IoS, this paper presents for the first time a compact dual-mode nested spherical resonator concept and a monolithic integration scheme using stereolithography apparatus (SLA). The proposed resonator concept is based on a hollow-metal sphere that is loaded by two dissimilar post-supported spheres which act as capacitive loads [17] that give rise to two independently-controlled modes. These modes have a significantly lower resonant frequency than those of a conventional hollow spherical single- or multi-mode resonator and can be exploited for the realization of compact single- [9] or dual-band BPFs. A similar post-loaded concept was demonstrated in [15], however for a cubical resonator and only for single-band transfer function as opposed to dual-band in this work.

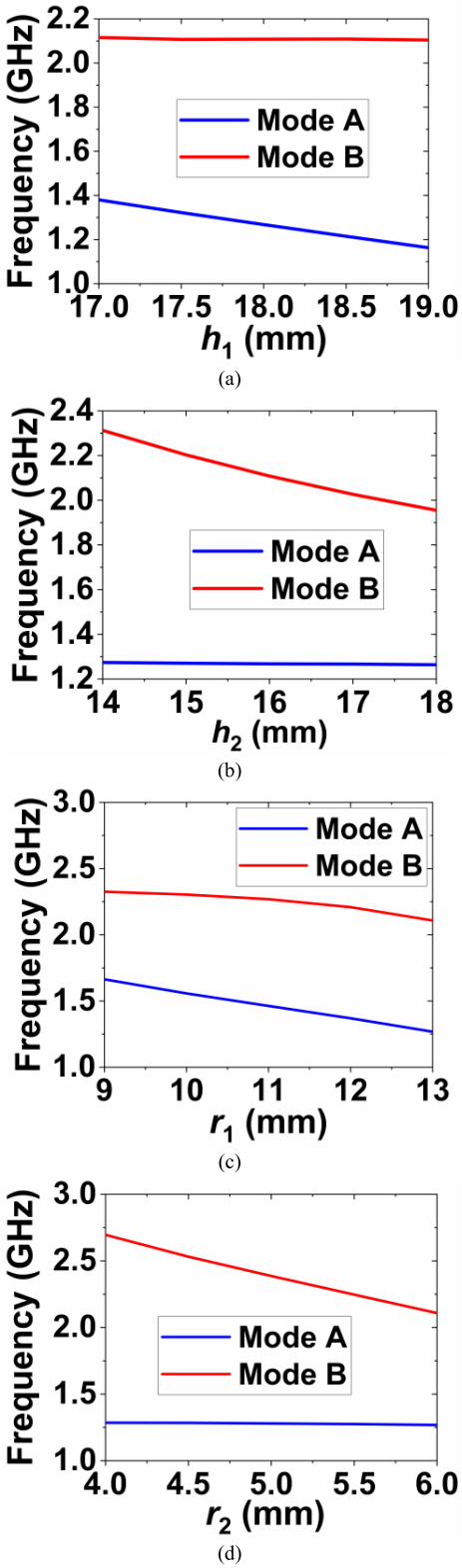

FIGURE 2. Resonant frequency of Mode A and Mode B as a function of: (a) h_1. (b) h_2. (c) r_1. (d) r_2. The dimensions of the resonator are: r_1 = 13 mm, r_2 = 6 mm, r_3 = 24 mm, h_1 = 18 mm, h_2 = 16 mm, rp_1 = 2 mm, rp_2 = 2.3 mm.

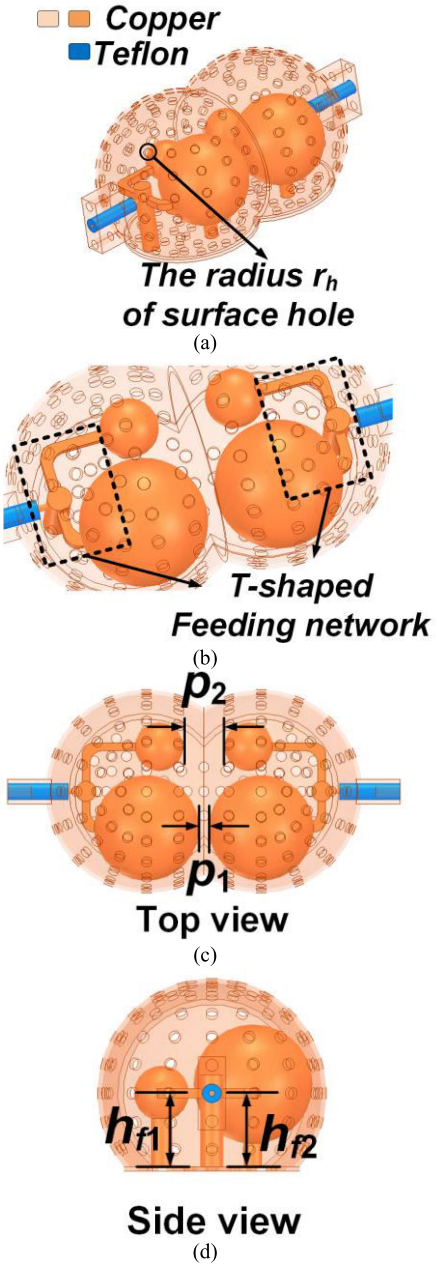

FIGURE 3. (a) Dual-band nested-spherical BPF. (b) Detail view of the T-shaped feeding network. (c) Top view. (d) Side view.

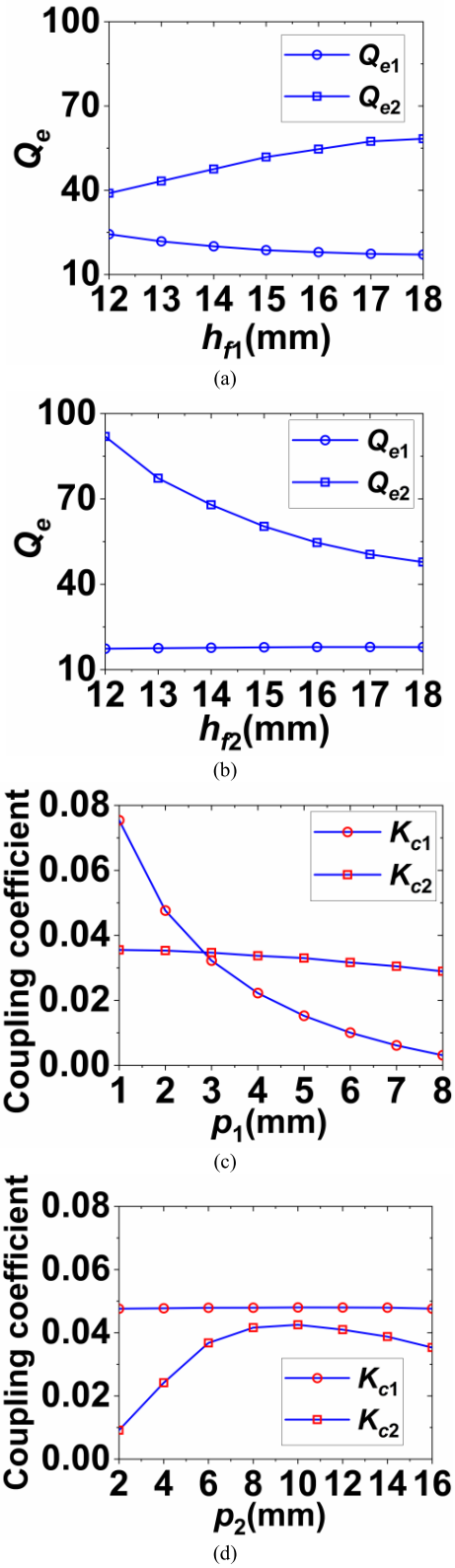

FIGURE 4. (a) Q_e for the low frequency band as a function of h_{f1}. (b) Q_e for the high frequency band as a function of h_{f2}. (c) K_{c1}, K_{c2} as a function of p_1. (d) K_{c1}, K_{c2} as a function of p_2.

Furthermore, the proposed dual-mode nested spherical resonator concept allows to independently adjust the bandwidth and the center frequency of each passband as unique advantages to be highlighted.

II. FILTER DESIGN AND ANALYSIS

A. NOVEL DUAL-MODE NESTED SPHERICAL RESONATOR

The 3D geometry of the dual-mode nested-spherical resonator is shown in Fig. 1(a) alongside the E-field distribution of its first two modes, namely Mode A and Mode B in Fig. 1(b) and Fig. 1(c) respectively. It comprises a nest of spheres, i.e., a hollow metallic sphere and two post-supported fully-metallic spheres that give rise to two

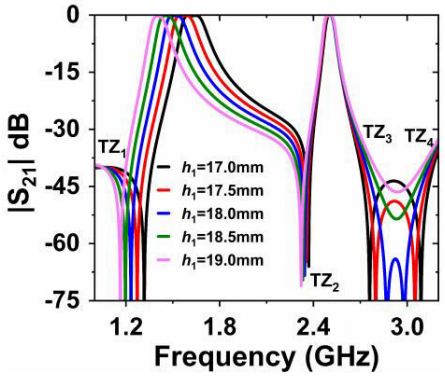

(a)

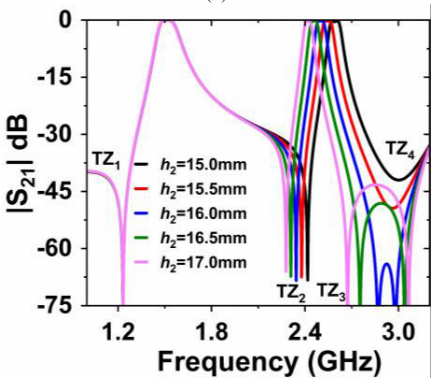

(b)

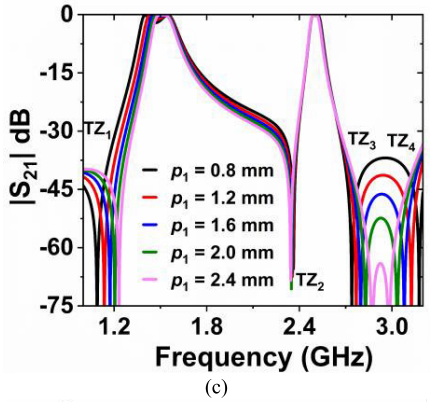

(c)

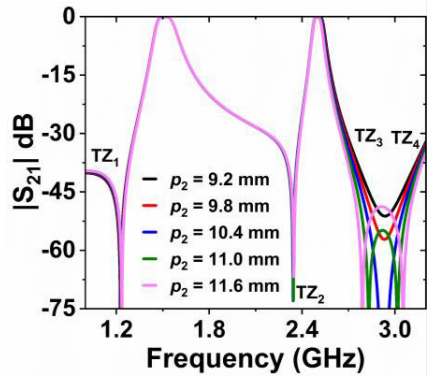

(d)

FIGURE 5. (a) Simulated |S21| as a function of h_1, (b) h_2, (c) p_1 and (d) p_2. In these examples: $r_1 = 13$ mm, $r_2 = 6$ mm, $r_3 = 24$ mm, $h_1 = 18$ mm, $h_2 = 16$ mm, $p_1 = 2.4$ mm, $p_2 = 10.2$ mm, $r_{p1} = 2$ mm, $r_{p2} = 2.3$ mm.

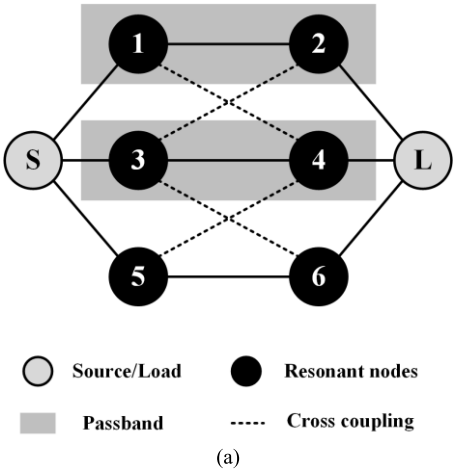

(a)

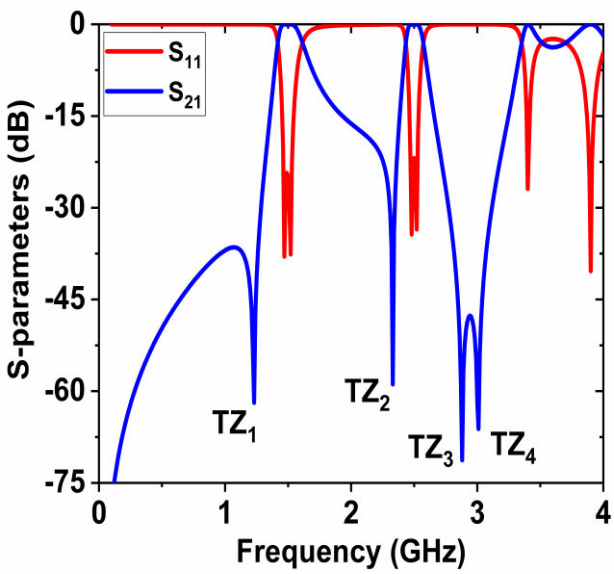

$$\begin{bmatrix} 0 & 0.33 & 0 & 0.21 & 0 & 0.254 & 0 & 0 \\ 0.33 & 1.35 & 0.12 & 0 & 0.25 & 0 & 0 & 0 \\ 0 & 0.12 & 1.35 & -0.25 & 0 & 0 & 0 & 0.33 \\ 0.21 & 0 & -0.25 & 0.17 & 0.045 & 0 & 0.198 & 0 \\ 0 & 0.25 & 0 & 0.045 & 0.17 & 0.198 & 0 & -0.21 \\ 0.254 & 0 & 0 & 0 & 0.198 & -0.65 & 0.18 & 0 \\ 0 & 0 & 0 & 0.198 & 0 & 0.18 & -0.65 & -0.254 \\ 0 & 0 & 0.33 & 0 & -0.21 & 0 & -0.254 & 0 \end{bmatrix}$$

(b)

FIGURE 6. (a) The coupling routing diagram, (b) Synthesized response, and coupling matrix of the dual-band BPF.

independently-controlled resonant modes. The bottom part of the sphere has been flattened to enhance mechanical stability of the post-loaded spheres and the external coupling structure using SLA 3D printing.

Table 1 depicts a comparison between the resonant frequencies and Q of the conventional spherical resonator and the proposed nested-spherical resonator. They have been obtained with eigenmode simulations. As shown, the resonant frequency of first four modes of the nested spherical resonator are significantly lower than those of the conventional hollow spherical resonator for the same outer radius. As such

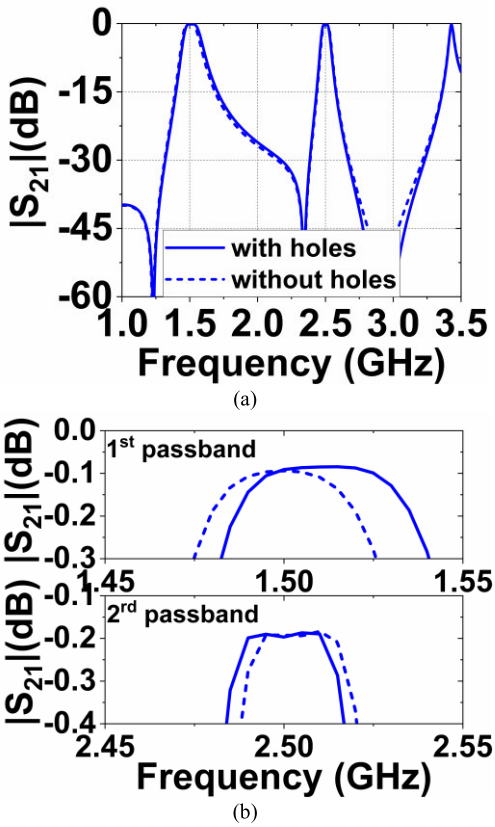

FIGURE 7. (a) EM-simulated response of the dual-band BPF in the absence and presence of Cu-platting holes with $r_h = 1.25$ mm (b) Detail of insertion loss zooming in each passband.

TABLE 2. Comparison with state-of-the-art 3-D printed dual-band filters.

Ref.	Ord.	R.T.	CF (GHz)	FBW (%)	RL (dB)	Q_{eff}	IL (dB)	Size (λ_0^3)
[7]	2	Sp./SLS	12.0/12.49	1/2	20/20	2176/1504	0.6/0.45	3.88
[8]	3	Sp./SLA	9.7/10.06	1/1.2	11/21	4680/5400	0.44/0.29	0.858
[13]	2	Co./SLA	3.7/4.2	8.1/4.3	12/22	800/1000	0.26/0.3	0.049
[13]	3	Co./SLA	3.7/4.0	4.9/3.3	14/>20	1020/1300	0.32/0.34	0.072
[14]	2	Co./SLA	3.34/5.04	11.1/2.6	>13	420/670	0.32/0.84	0.021
T.W.	2	Sp./SLA	1.5/2.47	8.13/2.87	16.5/17	1448/2088	0.14/0.39	0.0255

(Ref. = reference, Ord. = order, R.T. = resonator type, R.W. = rectangular waveguide, Co. = coaxial, Sp. = spherical, T.W. = this work)

they can be exploited for the realization of smaller filters. Furthermore, the resonant frequencies of first two modes (Mode A, B in Fig. 1) can be independently adjusted by changing the radius of each sphere (r_1 and r_2) or their distance from the bottom wall (h_1 and h_2) of the cavity as shown in Fig. 2.

B. DUAL-MODE DUAL-BAND FILTER

The dual-mode nested spherical resonators can be exploited for the realization of a dual-band second order BPF as shown in Fig. 3. The resonant modes of each resonator are excited through a T-shaped external coupling (Q_e) configuration that is directly attached to the SMA connector and on the spheres.

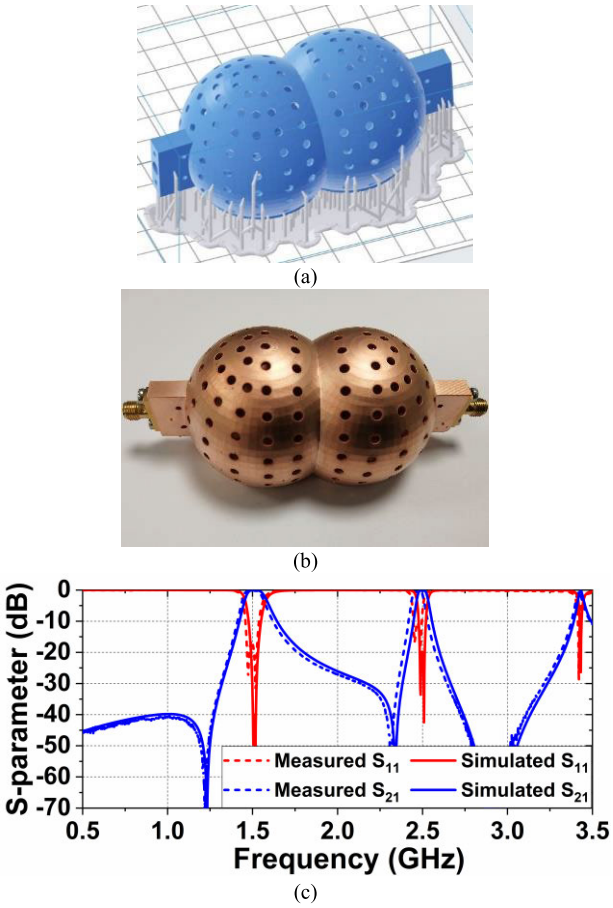

FIGURE 8. (a) CAD model for SLA-based monolithic manufacturing. (b) Prototype. The dimensions of the filter are: $r_1 = 6$ mm, $r_2 = 13$ mm, $r_3 = 24$ mm, $h_1 = 18$ mm, $h_2 = 16$ mm, $p_1 = 2.4$ mm, $p_2 = 10.2$ mm, $r_{p1} = 2$ mm, $r_{p2} = 2.3$ mm, $h_{f1} = h_{f2} = 15$ mm. (c) Simulated and measured S-parameters.

Furthermore, it is also connected to ground through a post to enhance mechanical stability. The Q_e for each band can be independently determined and controlled by altering the taping location (h_{f1} and h_{f2}) as shown in Fig. 4 (a), (b). Likewise, the inter-resonator coupling of the low (K_{c1}) and the high band (K_{c2}) can also be independently materialized and adjusted by the loading spheres spacing between the two resonators p_1 and p_2 as shown in Fig. 4(c), (d). The center frequency of two passbands can be modified by changing h_1 and h_2 as shown in Fig. 5(a) and (b) and the bandwidth of each band also can be controlled by altering p_1 and p_2 as depicted in Fig. 5(c) and (d). TZ_1 is due to the phase difference between coupling paths; TZ_2 is due to cross coupling between the different modes. TZ_3 and TZ_4 are due to destructive interference of the RF signals reaching the filter output through the higher-order modes as in any multi-mode filters. The location of the transmission zeros (TZs) can also be altered as shown in Fig. 5. Specifically, TZ_1 can be tuned by h_1 and h_2 and TZ_2 can reconfigured through h_1 and h_2 and TZ_3 and TZ_4 can be controlled by changing h_1, h_2, p_1 and p_2. Moreover, the coupling routing diagram of the filter is shown in Fig. 6(a) and the resonant nodes 1-4 are used in

this design and node 5-6 are higher-order modes. This is also demonstrated in the synthesized response of the corresponding coupling routing diagram of the filter in Fig. 6(b) below.

III. TEST RESULTS AND DISCUSSION

To validate the dual-band nested-spherical concept, a monolithic two-pole/four-TZ dual-band BPF geometry comprising of two nested-spherical resonators was designed for two frequency bands with the following characteristics: low band: f_{cen} = 1.52 GHz, FBW = 7.9 % and high band: f_{cen} = 2.5 GHz, FBW= 2.4 %. Manufacturing was accomplished with an SLA 3D printer and Cu metallization was performed using a commercially-available copper plating process with 50 μm copper thickness. The surface holes are needed to facilitate Cu-platting process of the SLA 3D printed filter that needs to be printed as fully-enclosed plastic structure. The diameter of the holes is selected so that they don't radiate at the center frequency and as such have no impact in the passband insertion loss as evidenced in Fig. 7. The CAD model for SLA manufacturing and the practical prototype are shown in Fig. 8(a) and (b), respectively. Higher order transfer functions can be implemented by cascading multiple dual-post spherical resonators through impedance inverters. The EM-simulated and RF-measured S-parameters of the proposed filter are shown in Fig. 8(c) and appear to be in a good agreement successfully-validating the proposed dual-mode nested-spherical resonator concept. Besides, the passband around 3.4 GHz is the higher order mode as evidenced in Fig. 6. The measured RF performance can be summarized as follows: low-frequency passband: f_{cen}: 1.5 GHz, FBW: 8.13 %, minimum IL: 0.14 dB, return loss (RL): > 16.5 dB, and effective Q factor (Q_{eff}) 1448, high-frequency passband: f_{cen}: 2.47 GHz, FBW: 2.87 %, minimum IL: 0.39 dB, RL > 10.7 dB, and Q_{eff}: 2088. A comparison with state-of-the-art 3D dual-band BPFs is depicted in Table 2. As shown, the proposed dual-band filter has lower IL and higher Q_{eff} than the majority of the reported 3D printed dual-band BPFs and especially the ones in [13] and [14]. Furthermore, the dual-mode nested-spherical resonator concept is uniquely shown in this work for the first time for the realization of compact dual-band BPFs.

IV. CONCLUSION

This paper reported on a new class of dual-band monolithically-integrated BPFs. They are based on a novel compact dual-mode nested-spherical resonator configuration that facilitates the realization of two independently-controlled resonant modes that can be exploited for dual-band BPF design. The proposed resonator geometry is composed of a spherical hollow air-filled cavity that is loaded with two post-supported metallic spheres that give rise to two independently-controlled resonant modes that resonate at significantly lower frequencies than a conventional hollow spherical resonator allowing for smaller filters to be realized. Further miniaturization is achieved through monolithic SLA-based integration. The proposed filter concept allows for versatile dual-band transfer function design whose bands can be independently controlled in terms of frequency and bandwidth.

REFERENCES

[1] Y. Wu and Q. Zeng, "A novel dual-band waveguide filter with multiple transmission zeros based on TE_{102}- and TE_{103}-modes," *IEEE Microw. Wireless Compon. Lett.*, vol. 32, no. 10, pp. 1159–1162, Oct. 2022.
[2] J. F. V. Sullca, S. Cogollos, M. Guglielmi, and V. E. Boria, "Dual-band filters in rectangular waveguide based on resonant apertures," in *IEEE MTT-S Int. Microw. Symp. Dig.*, Atlanta, GA, USA, Jun. 2021, pp. 192–195.
[3] M. H. Golzar and M. Memarian, "Orthogonal-mode dual-band rectangular waveguide filters," in *Proc. 27th Iranian Conf. Electr. Eng. (ICEE)*, Yazd, Iran, Apr. 2019, pp. 1534–1537.
[4] F.-C. Chen, J.-M. Qiu, S.-W. Wong, and Q.-X. Chu, "Dual-band coaxial cavity bandpass filter with helical feeding structure and mixed coupling," *IEEE Microw. Wireless Compon. Lett.*, vol. 25, no. 1, pp. 31–33, Jan. 2015.
[5] Y. Xie, F.-C. Chen, Q.-X. Chu, and Q. Xue, "Dual-band coaxial filter and diplexer using stub-loaded resonators," *IEEE Trans. Microw. Theory Techn.*, vol. 68, no. 7, pp. 2691–2700, Jul. 2020.
[6] Z.-C. Zhang, H.-J. Li, X.-Z. Yu, Y. He, and S.-W. Wong, "Dual-narrowband/wideband filters using modified coaxial cavities with large frequency ratios," *IEEE J. Microw.*, vol. 2, no. 4, pp. 690–698, Oct. 2022.
[7] Y. Chen, G. Zhang, J. Hong, Z. Sun, J. Yang, W. Tang, and C. Feng, "3-D printed dual-band filter based on spherical dual-mode cavity," *IEEE Microw. Wireless Compon. Lett.*, vol. 31, no. 9, pp. 1047–1050, Sep. 2021.
[8] E. López-Oliver and C. Tomassoni, "Dual-band filters based on dual-mode ellipsoidal cavities," in *IEEE MTT-S Int. Microw. Symp. Dig.*, Denver, CO, USA, Jun. 2022, pp. 88–91.
[9] J. Liu, K. Zhao, and D. Psychogiou, "Miniaturized monolithic 3-D printed bandpass filters using nested spherical resonators," *IEEE Trans. Compon., Packag., Manuf. Technol.*, vol. 13, no. 9, pp. 1461–1470, Sep. 2023.
[10] Y. Li, J. Li, M. Zhang, H. Wang, J. Xu, and S. Xiao, "A monolithic stereolithography 3-D printed Ka-band spherical resonator bandpass filter," in *Proc. IEEE Radio Wireless Symp. (RWS)*, Jan. 2018, pp. 56–59.
[11] F. Zhang, S. Gao, J. Li, Y. Yu, C. Guo, S. Li, M. Attallah, X. Shang, Y. Wang, M. J. Lancaster, and J. Xu, "3-D printed slotted spherical resonator bandpass filters with spurious suppression," *IEEE Access*, vol. 7, pp. 128026–128034, 2019.
[12] J. Li, G. Huang, and T. Yuan, "Monolithic 3-D printed spherical-resonator-based olympic-topology bandpass filters," in *Proc. IEEE Int. Symp. Antennas Propag. USNC/URSI Nat. Radio Sci. Meeting*, Jul. 2018, pp. 1441–1442.
[13] K. Zhao and D. Psychogiou, "Monolithic multiband coaxial resonator-based bandpass filter using stereolithography apparatus (SLA) manufacturing," *IEEE Trans. Microw. Theory Techn.*, vol. 70, no. 9, pp. 4156–4166, Sep. 2022.
[14] K. Zhao and D. Psychogiou, "Monolithically-integrated 3D printed coaxial bandpass filters and RF diplexers: Single-band and dual-band," *Int. J. Microw. Wireless Technol.*, vol. 14, no. 3, pp. 293–304, Apr. 2022.
[15] P. Vaitukaitis, K. Nai, and J. Hong, "A versatile 3-D printable model for implementing multiband waveguide filters with flexible filtering characteristics," *IEEE Access*, vol. 11, pp. 110051–110059, 2023.
[16] P. Vaitukaitis, K. Nai, and J. Hong, "Investigation of metal 3-D printed high-Q multiband waveguide filters using spherical resonators," *IEEE Access*, vol. 12, pp. 1497–1507, 2024.
[17] D. Sh-Asanjan and R. R. Mansour, "A novel coaxial resonator for high power applications," in *Proc. 44th Eur. Microw. Conf.*, Rome, Italy, Oct. 2014, pp. 295–298.

JIAWEI LIU (Graduate Student Member, IEEE) received the bachelor's degree in electrical engineering from Southwest Minzu University, Chengdu, China, in 2017. He is currently pursuing the Ph.D. degree in electrical engineering with the University of Electronic Science and Technology of China (UESTC), Chengdu, China.

His main research interests include RF/microwave and mm-wave circuits and systems.

DIMITRA PSYCHOGIOU (Senior Member, IEEE) received the Dipl.-Eng. degree in electrical and computer engineering from the University of Patras, Patras, Greece, in 2008, and the Ph.D. degree in electrical engineering from the Swiss Federal Institute of Technology (ETH), Zürich, Switzerland, in 2013.

She is currently a Professor of electrical and electronic engineering with University College Cork (UCC), Ireland, and the Head of the Advanced RF Technology Group, Tyndall National Institute, Cork, Ireland. Prior to joining UCC, she was a Senior Research Scientist with Purdue University, West Lafayette, IN, USA, and an Assistant Professor with the University of Colorado at Boulder, Boulder, CO, USA. Her current research interests include RF design and characterization of reconfigurable microwave and millimeter-wave passive components, RF-MEMS, acoustic wave resonator-based filters, tunable filter synthesis, frequency-agile antennas, and additive manufacturing (AM) technologies for 3D antenna subsystems. She is a Senior Member of the International Union of Radio Science (URSI) and a member of the IEEE MTT-S Filters and Passive Components (MTT-5) and Microwave Control Materials and Devices (MTT-13) Committees. She has received the 2021 Roberto Sorrentino Prize, the SFI Research Professorship Award, the 2020 NSF CAREER Award, the 2020 URSI Young Scientist Award, and the Junior Faculty Outstanding Research Award from UC Boulder. She serves on the Technical Review Board of various IEEE and EuMA conferences and journals. She is the Chair of MMT-13 and a Secretary of USNC-URSI Commission D. She is an Associate Editor of the IEEE Microwave and Wireless Components Letters and the *International Journal of Microwave and Wireless Technologies*. Previously, she was an Associate Editor of the *IET Microwaves, Antennas and Propagation journal*.